Scientific Reports

https://doi.org/10.1038/s41598-026-42423-0

Article in Press

# Femoral finite element analysis of a novel cementless revision total knee arthroplasty system

Received: 14 November 2025

Accepted: 25 February 2026

Published online: 13 March 2026

Cite this article as: Dong Z., Wang X., He D. *et al.* Femoral finite element analysis of a novel cementless revision total knee arthroplasty system. *Sci Rep* (2026). https://doi.org/10.1038/s41598-026-42423-0

Ziyang Dong, Xinguang Wang, Dongyang He, Xiaofan Lv, Ti Zhang, Zijian Li, Xiaogang Zhang & Hua Tian

# Femoral finite element analysis of a novel cementless revision total knee arthroplasty system

Ziyang Dong[1,2*], Xinguang Wang[1,2*], Dongyang He[3], Xiaofan Lv[3], Ti Zhang[1,2], Zijian Li[1,2], Xiaogang Zhang[3#], Hua Tian[1,2#]

* Ziyang Dong and Xinguang Wang contribute equally to this article.

# Xiaogang Zhang and Hua Tian are co-corresponding authors in this article.

1. Department of Orthopaedics, Peking University Third Hospital, Beijing, China
2. Engineering Research Center of Bone and Joint Precision Medicine, Ministry of Education, Beijing, China
3. School of Mechanical Engineering, Southwest Jiaotong University, Chengdu, Sichuan province, China

**Corresponding Author:**

Hua Tian, Department of Orthopaedics, Peking University Third Hospital, tianhua@bjmu.edu.cn

Xiaogang Zhang, School of Mechanical Engineering, Southwest Jiaotong University, xg@swjtu.edu.cn

**Abstract**

**Background**: Revision total knee arthroplasty (RTKA) is a highly complex procedure challenged by bone defects and compromised biomechanical stability, which may threaten implant fixation and long-term survivorship. This study aimed to introduce a novel cementless RTKA system and evaluate the resulting femoral initial stability.

**Method**: A novel cementless femoral RTKA system based on metaphyseal and biological fixation, comprising a femoral condyle component, metaphyseal cone, and optional intramedullary stems and metal augments, was evaluated using finite element analysis. The initial stability of the system was assessed in a CT-based femoral model under conditions with or without bone defects, at different defect locations, and with or without the use of intramedullary stems and metal augments.

**Results**: Finite element analysis demonstrated that, regardless of the presence of femoral bone defects, the system exhibited favorable interface micromotion and femoral stress distribution, indicating acceptable initial femoral stability. Intramedullary stems reduced micromotion but decreased the proportion of stress within the

reference range, whereas metal augments produced only limited numerical improvement without being essential for initial stability.

**Conclusion**: Within the investigated finite element model, the novel cementless RTKA system achieved acceptable initial femoral mechanical stability, even in the presence of femoral bone defects. Adequate initial stability could be obtained through metaphyseal fixation alone, while the additional use of intramedullary stems or metal augments provided limited incremental benefit.

**Keywords**: Revision total knee arthroplasty; Cementless fixation; Metaphyseal fixation; Finite element analysis

## Background

With the increasing application of primary total knee arthroplasties (TKAs) worldwide, the number of revision surgeries performed owing to TKA failure have increased significantly [1]. More than 200,000 revision total knee arthroplasties (RTKAs) are estimated to be performed annually in the US by 2030 [2], which will place a heavy burden on both patients and the healthcare system.

Bone defects - which are associated with aseptic loosening, infection, and improper removal of prostheses [1,3] - present a significant challenge in RTKA that cannot be ignored. Severe bone defects may affect the stability of the prosthesis and increase the complexity of RTKA [4,5]; thus, the management of bone defects is crucial in RTKA. To repair bone defects and reconstruct stability in RTKA, several techniques, including cementation, metal augmentation, intramedullary stem, bone grafting, and metaphyseal cones or sleeves, have been adopted depending on the location and severity of bone defects [5–7].

The Anderson Orthopedic Research Institute (AORI) classification is commonly used to report bone defects of varying severities and locations [4]. In AORI type II or III bone defects, the epiphyseal and metaphyseal bones are affected, presenting significant complexity in bone repair. Fixation of the epiphyseal zone alone may be

insufficient in the presence of severe bone defects and may lead to mechanical failure. Therefore, the use of metaphyseal fixation, where the bone is well-vascularized, conducive to osseointegration, and usually not completely damaged, has gained increasing attention [8]. Metaphyseal fixations, such as those using metaphyseal cones or sleeves, are designed to improve construct stability during the treatment of severe bone defects in RTKA [1,8]. Additionally, with the development of 3D printing, cones or sleeves with 3D printed porous surfaces could further improve bone ingrowth and long-term stability, making it possible to use a fully cementless prosthesis [9,10].

Despite these advances, the fixation strategy of current RTKA systems remains predominantly cemented or hybrid, whereas fully cementless revision constructs are rarely used in routine practice. Cemented fixation can provide reliable immediate stability; however, it is highly dependent on the integrity of the cement-bone interface and is associated with potential drawbacks, including cement fatigue, wear particles, and thermal injury [11,12]. These limitations may compromise long-term implant survivorship. In contrast, biologic fixation based on osseointegration has the potential to achieve durable long-term stability without the inherent disadvantages of bone cement [13]. Therefore, there is a clinical need for a novel

RTKA system that integrates the mechanical advantages of metaphyseal fixation with the concept of fully cementless biologic fixation. Based on this rationale, we designed a new cementless RTKA system featuring 3D-printed porous metaphyseal cones and other modular components, aiming to enhance initial stability, promote bone ingrowth, and ultimately improve long-term outcomes.

***Research Objective:*** This study aimed to verify the initial stability of the femoral components in this novel cementless RTKA system, determine the contribution of an intramedullary stem and metal augment at different locations of bone defects, and offer insights for their clinical application.

## Materials and methods

### *Finite element model of femur*

A 3D computer-aided design (CAD) model of the right femur was obtained using computed tomography (CT) data from a 66-year-old woman diagnosed with knee osteoarthritis. The slice thickness on the CT scan was 0.6 mm.

### *Femoral design of cementless RTKA system*

The novel femoral cementless RTKA system includes a femoral condylar component, a femoral metaphyseal cone, and an optional intramedullary stem and metal augment. Based on the concept of metaphyseal fixation, the outer contour of the femoral metaphyseal

cone was designed according to the inner contour of the femur, particularly in the metaphyseal zone, where a press fit could be achieved for solid fixation. The femoral metaphyseal cone was distally locked to the femoral condyle prosthesis with an adaptor, whereas it was proximally combined with an optional intramedullary stem through a threaded connection (Figure 1). In addition, the interface between the prosthesis and the bone features a 3D-printed trabecular structure that promotes bone tissue ingrowth and integration.

***Femur-prosthesis assembly***

The femoral components, tibial insert, and femur models were subjected to simulated bone resection and femur-prosthesis assembly. To simulate the axial loading on the mid-femur, the femur was cut along the middle section while preserving the distal portion. Femoral sectioning and surgical positioning of the prosthesis were performed by experienced orthopedic surgeons based on different bone defect locations and the presence of stems and augments. (Figure 2)

***Definition of bone defect***

The femoral bone defect in this study was defined as 15 mm in the distal femur and 10 mm in the posterior femur. These values correspond to structural defects commonly encountered in RTKA

that typically require augmentation or metaphyseal fixation. According to the AORI classification, such defect depth may correspond to type IIa or type IIb defects. The simulated patterns (medial, lateral, and combined medial-lateral bone loss) were designed to mimic common revision scenarios such as posteromedial deficiency, large single-condyle loss, and symmetric bicondylar loss, thereby enhancing the clinical relevance of the finite element models.

***Configuration setup***

First, two finite element models were created based on the presence of stems and the absence of bone defects (configuration 1 and 2). Second, another 12 finite element models were created based on three different bone defect locations (medial, lateral, and medial-lateral), the presence of stems, augments and femoral bone defects (configuration 3-14).



The details of the configurations are presented in table 1. D0/15 indicates a distal femoral bone defect with a depth of 0 or 15 mm, and P0/10 indicates a posterior femoral bone defect with a depth of 0 or 10 mm. M, L, and ML denote medial, lateral, and combined medial-lateral defect locations, respectively. A1/A0 indicate the presence or absence of a metal augment, and S1/S0 indicate the presence or absence of an intramedullary stem.

**Table 1.** Configuration setup

| | Configuration | Bone defect of the distal femur (mm) | Bone defect of the posterior femur (mm) | Location | Augment | Stem |
|---|---|---|---|---|---|---|
| 1 | D0-P0-S1 | 0 | 0 | - | - | + |
| 2 | D0-P0-S0 | 0 | 0 | - | - | - |
| 3 | D15-P10-A1-S1-M | 15 | 10 | medial | + | + |
| 4 | D15-P10-A1-S1-L | 15 | 10 | lateral | + | + |
| 5 | D15-P10–A0-S1-M | 15 | 10 | medial | - | + |
| 6 | D15-P10–A0-S1-L | 15 | 10 | lateral | - | + |
| 7 | D15-P10-A1-S0-M | 15 | 10 | medial | + | - |
| 8 | D15-P10–A1-S0-L | 15 | 10 | lateral | + | - |
| 9 | D15-P10–A0-S0-M | 15 | 10 | medial | - | - |
| 10 | D15-P10–A0-S0-L | 15 | 10 | lateral | - | - |
| 11 | D15-P10-A1-S1-ML | 15 | 10 | medial-lateral | + | + |
| 12 | D15-P10-A0-S1-ML | 15 | 10 | medial-lateral | - | + |
| 13 | D15-P10-A1-S0- | 15 | 10 | medial- | + | - |

| | | | | | | |
|---|---|---|---|---|---|---|
| | ML | | | lateral | | |
| 14 | D15-P10-B0-S0-ML | 15 | 10 | medial-lateral | - | - |

***Mesh Generation, material characteristics, and boundary conditions***

Finite element analysis was conducted using the ABAQUS software (Dassault Systèmes, France; version 2021; https://www.3ds.com/products/simulia/abaqus/). The resected femur and prosthesis solid model were imported into HYPERMESH 20.0 (Altair □ USA) for finite element mesh generation of the femur-prosthesis assembly. A mesh sensitivity analysis was conducted to determine the optimal element size, and the results were exported as ".inp" files. The femur consisted of trabecular and cortical bones. The outer surface of the femur was offset inward by 2.5 mm to divide it in two parts. The characteristics of these materials are listed in Table 2.



**Table 2.** Characteristic of materials

| **Component** | **Material** | **Modulus of Elasticity (MPa)** | **Poisson's ratio** |
|---|---|---|---|
| Femoral condyle component | CoCrMo | 210000 | 0.3 |

| | | | |
|---|---|---|---|
| Femoral metaphyseal cone | Ti6Al4V | 110000 | 0.3 |
| Mesh layer of the femoral condyle component | CoCrMo | 210000 | 0.3 |
| Mesh layer of the femoral metaphyseal cone | porous Ti6Al4V | 2400 | 0.3 |
| Intramedullary stem | Ti6Al4V | 110000 | 0.3 |
| Metal augment | porous Ti6Al4V | 2400 | 0.3 |
| Tibial insert | UHMWPE | 1016 | 0.46 |
| Cortical bone | - | 11000 | 0.3 |
| Trabecular bone | - | 400 | 0.3 |



Surface-to-surface contact pairs were established between the femur and implant components using a penalty contact formulation. All contact parameters and friction coefficients were adopted from previously published finite element and biomechanical studies to ensure physiologically reasonable model settings. A friction coefficient of 0.4 was assigned for the general implant-bone interfaces, while the articulation between the femoral component and the tibial insert was modeled with a coefficient of 0.04, as commonly adopted in knee arthroplasty finite element models [14]. The interfaces between the porous cone mesh layer-femur and the metal augment-femur were defined as frictional contacts with a

relatively high coefficient (μ = 1.0) [15], consistent with literature reporting high-friction behavior for porous metal structures in contact with bone.

Detailed information regarding contact between each pair is presented in Table 3. The porous layer on the femoral condylar component is extremely thin relative to its solid geometry, and reliable material properties for porous CoCrMo are not well established in previous literatures, as a result, the mesh layer of femoral condylar component was approximated as a simplified solid layer rather than explicitly modeling individual pores.

**Table 3.** Information regarding contact between components

| **Interface** | **Contact** | **Friction coefficient** |
|---|---|---|
| Femoral condyle component – femoral metaphyseal cone | bonded contact | - |
| Femoral condyle component - femoral condyle mesh layer | bonded contact | - |
| Femoral metaphyseal cone - femoral cone mesh layer | bonded contact | - |
| Metal augment - femoral condyle mesh layer | bonded contact | - |
| Intramedullary stem- femoral metaphyseal | bonded contact | - |

| | | |
|---|---|---|
| cone | | |
| Femoral metaphyseal cone mesh layer - femur | frictional contact | 1.0 |
| Femoral condyle component mesh layer - femur | frictional contact | 0.4 |
| Metal augment - femur | frictional contact | 1.0 |
| Intramedullary stem - femur | frictional contact | 0.4 |
| Femoral condyle component - tibial insert | frictional contact | 0.04 |



***Load application***

An axial load of 2030 N is applied to the mid-femur. The femoral prosthesis was in contact with the underlying tibial insert, and the load distribution was set to 60% on the medial condyle and 40% on the lateral condyle. A rotational force of 7 Nm was applied from the medial to the lateral side through the tibial insert to the femoral prosthesis. The proximal cut surface of the mid-femur was fully constrained in all degrees of freedom to prevent rigid body motion. These applied loads are representative of a normal physiological loading condition during walking at the stance phase before toe-off,

and similar boundary conditions have been validated in previous finite element and biomechanical studies [16].

***Mesh sensitivity analysis***

The femur and prosthesis models were meshed in HYPERMESH, and the appropriate mesh size was determined based on the results of the mesh sensitivity analysis. Herein, element sizes of 2 mm, 1.5 mm, and 1 mm were selected for the sensitivity analysis. The criteria for mesh convergence were the maximum von Mises stress and maximum micromotion at the interface.

The numbers of elements for the femur and femoral stem at different mesh sizes are listed in Table 4. The results indicated that when the mesh size was reduced from 1.5 mm to 1 mm, the change in the maximum von Mises stress and maximum micromotion was less than 5%, demonstrating that the mesh sensitivity results converged.



**Table 4.** Mesh sensitivity analysis.

| **Size (mm)** | **Cortical** | **Trabecular** | **Metaphyseal cone** | **Porous layer of the metaphyseal cone** | **Implant** | **Stem** | **Insert** | **Max von Mises (MPa)** | **Maximum Micromotion (μm)** | **Error (%)** |
|---|---|---|---|---|---|---|---|---|---|---|
| 1.0 | 24410 | 621927 | 107587 | 30969 | 27292 | 3273 | 1651 | 124.19 | 20.02 | - |

| | | | | | | | | | | |
|---|---|---|---|---|---|---|---|---|---|---|
| | 0 | | | | 0 | 7 | 12 | | | |
| 1.5 | 77411 | 310243 | 31851 | 14573 | 74069 | 10605 | 50981 | 122.80 | 19.27 | 3.75 |
| 2.0 | 31183 | 232096 | 15777 | 8487 | 34165 | 49613 | 22052 | 132.07 | 17.30 | 10.22 |

***Finite element model validation***

The predicted maximum von Mises stress in the femur was 36.81 MPa, which is comparable in magnitude to values reported in previous finite element studies of distal femoral reconstruction [17,18]. In addition, the stress was mainly distributed in the medial cortical bone, consistent with the physiological load transfer characteristics of the femur. Furthermore, the contact stress on the tibial insert was also analyzed. The predicted maximum contact stress was 59.57 MPa, which is similar in magnitude to values reported in previous finite element studies [19,20]. These findings indicate that the model provides a reasonable representation of the mechanical behavior of the femoral RTKA system.

***Assessment parameters and interpretation criteria***

The assessment parameters of this study were the interface micromotion between bone and implant and the von Mises equivalent stress of the femur. Maximum micromotion at the bone-

implant interface was compared with the commonly cited safety upper limit of 150 μm [16,21]. Micromotions below this limit are generally regarded as indicative of acceptable initial mechanical stability, whereas values exceeding this level may imply a potential risk of mechanical loosening. For stress evaluation, this study focused primarily on the proportion of cancellous bone elements within the reference stress interval of 0.1-2.8 MPa [22]. According to previous reports, stresses <0.1 MPa may be related to insufficient mechanical stimulation and possible stress shielding, while stresses >2.8 MPa may indicate potential localized overload [22]. Calculating the percentage of bone volume within this interval provides a global assessment of load transfer characteristics and the mechanical environment of cancellous bone.

## Results

### *Femoral initial stability and effects of intramedullary stems without bone defects*

*Interface micromotion*

In the absence of additional femoral bone defects, comparison of the two models (D0S1: intact femur, with stem; D0S0: intact femur, without stem) demonstrated that the intramedullary stem markedly reduced micromotion at the cone-bone interface from 49.71 μm to 7.81 μm (table 5), representing a numerical improvement.

Importantly, however, micromotions in both the stemmed and stemless configurations remained well below the commonly accepted safety upper limit of 150 μm, indicating acceptable initial mechanical stability even without stem fixation. In contrast, the stem had little influence on micromotion at the interface between the distal femoral condylar component and the femur (figure 3).

*von Mises equivalent stress*

In case of a femur without additional bone defects, the stress distribution diagram showed that the maximum von Mises equivalent stress in the femur with the stem was similar to that in the femur without the stem. The proportion of von Mises equivalent stresses in the reference range of the cancellous bone (0.1-2.8 MPa) were 85.44% and 76.71% in the stemless and stem configurations, respectively (figure 3, table 5).



**table 5.** Analysis of micromotion and von Mises stress in different configurations

| | **No bone defect** | | **Medial bone defect** | | **Medial-lateral bone defect** | | **Lateral bone defect** | |
|---|---|---|---|---|---|---|---|---|
| **Configuration** | **Stem** | **Stemless** | **Stem** | **Stemless** | **Stem** | **Stemless** | **Stem** | **Stemless** |
| Maximum micromotion | 7.81 | 49.71 | 10.27 | 55.29 | 9.87 | 54.89 | 8.20 | 48.79 |

| | | | | | | | | |
|---|---|---|---|---|---|---|---|---|
| (μm) | | | | | | | | |
| Maximum von Mises stress （MPa） | 36.81 | 36.89 | 66.46 | 71.86 | 39.44 | 43.83 | 37.96 | 38.30 |
| Proportion within the reference von Mises stress range | 76.71 % | 85.44 % | 74.61% | 82.67% | 89.09% | 94.16% | 88.73% | 93.64% |
| **Configuration** | **-** | **-** | **Augment** | **No augment** | **Augment** | **No augment** | **Augment** | **No augment** |
| Maximum micromotion (μm) | - | - | 46.05 | 55.29 | 51.67 | 54.89 | 49.83 | 48.79 |
| Maximum von Mises stress （MPa） | - | - | 44.87 | 71.86 | 39.93 | 43.83 | 38.31 | 38.30 |
| Proportion within the reference von Mises stress range | - | - | 84.03% | 82.67% | 93.62% | 94.16% | 93.58% | 93.64% |



***Effects of intramedullary stem on initial stability with bone defects***

*Interface micromotion*

The corresponding finite element models included three defect locations (medial, lateral, and combined medial-lateral defects), with and without stem implantation, resulting in six configurations in

total (D15-P10-A0-S0-ML vs. D15-P10-A0-S1-ML; D15-P10-A0-S0-M vs. D15-P10-A0-S1-M; D15-P10-A0-S0-L vs. D15-P10-A0-S1-L).

When the femur exhibited bone defect (15 mm in distal femur and 10 mm in posterior femur) in three different locations, the presence of the stem numerically reduced the maximum micromotion at the interface between the mesh layer of the femoral metaphyseal cone and the femur (from 54.89 μm to 9.87 μm for medial-lateral bone defects; from 55.29 μm to 10.27 μm in medial bone defects; and from 48.79 μm to 8.20 μm in lateral bone defects). The maximum micromotions were ranked according to the location of the bone defect from the highest to the lowest as follows: medial > medial-lateral > lateral (figure 4, table 5).

*von Mises equivalent stress*

In all three bone-defect scenarios, the maximum equivalent stress of the femur without a stem was slightly higher than that in the stemmed configuration. The maximum equivalent stresses were ranked according to the location of the bone defect from the highest to lowest as follows: medial > medial-lateral > lateral. However, the proportion of stress falling within the reference range of 0.1-2.8 MPa in all the three areas of bone defects was consistently greater in the absence of stems. (Figure 4 and Table 5)

***Effects of metal augments on the initial stability with bone***

***defects***

*Interface micromotion*

The corresponding finite element models included three defect locations (medial, lateral, and combined medial-lateral defects), with and without augment, comprising six configurations (D15-P10-A0-S0-ML vs. D15-P10-A1-S0-ML; D15-P10-A0-S0-M vs. D15-P10-A1-S0-M; D15-P10-A0-S0-L vs. D15-P10-A1-S0-L).

When the femur exhibited additional bone defects (15 mm in distal femur or 10 mm in posterior femur), the presence of augments resulted in a mild reduction in the maximum micromotion at the interface between the mesh layer of the metaphyseal cone and the femur in cases of medial bone defects (from 55.29 μm to 46.05 μm). However, for medial-lateral and lateral bone defects, augments had minimal impact on the maximum micromotion. (Figure 5)



*von Mises equivalent stress*

When the femur exhibited additional bone defects in the medial condyle, the stress distribution showed that the femur without augments had a numerically higher maximum von Mises equivalent stress. For medial-lateral and lateral bone defects, the stresses were similar regardless of the presence of augments. The maximum stress was ranked according to the location of the bone defect from highest to lowest as follows: medial > medial-lateral > lateral. In addition,

under different bone-defect locations, the use of augments showed little effect on the proportion of femoral equivalent stress within the reference range. (Figure 5 and Table 5).

## Discussion

The management of bone defects and prosthetic initial stability are crucial determinants of postoperative outcomes in RTKA patients. These demands place higher requirements on the design and fixation strategy of revision prostheses. A finite element analysis based on the novel cementless RTKA system was conducted to evaluate its femoral initial stability. Within the investigated finite element models and loading conditions, acceptable initial femoral stability was observed across the examined configurations, both with and without femoral bone defect, and regardless of the use of an intramedullary stem or metal augment.

### *Cementless and metaphyseal fixation in the novel RTKA system*

In this novel RTKA system, a fully cementless femoral fixation concept was adopted, in which all major components including the femoral condyle, metaphyseal cone, stem, and augment are designed for cementless fixation rather than relying on hybrid cemented fixation.

Another key feature of this system is the integration of metaphyseal

fixation philosophy into the femoral design. The metaphysis is considered a crucial zone in RTKA fixation, as the bone in this region is often relatively preserved and suitable for biological ingrowth [23,24]. The femoral metaphyseal cone in this system serves as the primary load-bearing structure, aiming to provide reliable initial mechanical stability while establishing a favorable environment for long-term biological fixation.

In RTKA, 3D-printed cones or sleeves are reported as a novel and effective technique for managing bone defects in previous literatures [25–27]. The present system, however, is not limited to a single cone component, but represents a comprehensive modular platform in which the femoral condyle component, metaphyseal cone, stem, and augment are designed to function as an integrated construct with dedicated instrumentation. Within this system, the cone serves not only to reconstruct metaphyseal bone defects, but also to act as the primary metaphyseal fixation element, providing initial stability and a foundation for biological ingrowth.

***Femoral initial stability of the RTKA system without bone defects***

Initial stability is crucial for the survival of revision prostheses and clinical outcomes, especially in cases of large bone defects. Previous studies based on finite element analyses and biomechanical testing

have demonstrated the beneficial effects of metaphyseal fixation in providing reliable initial stability for revision implants [16,28,29].

In the present study, we further evaluated this concept within the current femoral RTKA system, focusing on its ability to achieve adequate stability under various configurations. Across all configurations analyzed in this study, the maximum interface micromotions remained below 150 μm, and the majority of femoral bone stresses were distributed within the reported reference range. Based on the present finite element findings, these results indicate that this novel femoral RTKA system is capable of providing favorable initial stability, supporting the feasibility of the proposed cementless metaphyseal fixation concept.

***Clinical relevance of the simulated defect model***

The bone defects modeled in this study represent femoral deficiencies that directly challenge implant fixation in RTKA rather than minor contained defects. Loss of distal and posterior condylar support alters the load-sharing pattern between the femoral component and host bone, making the construct more dependent on metaphyseal fixation. Evaluating such bone defects is therefore essential to understand whether a cone-based cementless system can provide reliable initial stability under compromised conditions.

In our clinical experience, we frequently encountered residual bone

defects after standard preparation and trial implantation. These situations commonly raise two practical questions: whether the asymmetry of the bone defect necessitates an intramedullary stem to enhance overall stability and load transfer, and whether the remaining bone defect should be filled with additional metal augments. The present finite element analysis was interpreted in this context, and the application of intramedullary stems and metal augments under bone defect conditions was further analyzed and discussed.

***The effects of intramedullary stem in bone defects***

Intramedullary stems have been widely used in RTKA, as they are designed to transfer and redistribute loads from compromised metaphyseal bone to the relatively intact diaphysis, thereby contributing to load sharing, optimization of stress transfer, and enhancement of overall fixation stability [30]. However, the use of intramedullary stems may also be associated with potential drawbacks, including additional stem tip pain, intra-operative periprosthetic fractures and stress shielding effects [31–33]. In addition, effective metaphyseal fixation alone may partially contribute to stress transfer and load distribution, thereby reducing the dependence on diaphyseal stem fixation in certain configurations[34]. Fonseca et al.[16] demonstrated that when

metaphyseal sleeve fixation is used, satisfactory initial stability can be achieved without a diaphyseal stem, and the additional use of a stem is not mandatory from a biomechanical perspective.

In the present study, although the application of stem markedly reduced the maximum micromotion of bone-implant interface, the stemless configuration already satisfied the safety criterion. However, the proportion of femoral bone stress within the reference range of 0.1-2.8 MPa was lower in the stemmed configurations. Specifically, the use of an intramedullary stem was associated with an increased proportion of low-stress regions (<0.1 MPa) in the femur, increasing from 14.50% to 22.42% in the absence of bone defects, from 17.20% to 24.88% in medial defects, from 5.63% to 10.25% in combined medial-lateral defects, and from 6.27% to 10.83% in lateral defects. The increase in low-stress regions is likely attributable to the load transfer and redistribution effect of the intramedullary stem. Excessively low stress levels (<0.1 MPa) may reduce local mechanical stimulation of the femoral bone and are associated with potential stress shielding and bone resorption risks, which could adversely affect long-term fixation [35].

Therefore, based on the present finite element findings, the additional biomechanical benefit of routine intramedullary stem use in this cementless revision system appears limited, and further

experimental and clinical validation is warranted.

***The effects of metal augments in bone defects***

Metal augment is an important option for managing femoral bone defects in RTKA, offering advantages such as modularity and surgical flexibility[36]. In the present revision system, cementless 3D-printed porous augments were used, which are designed to restore bone defects while also facilitating bone ingrowth. Innocenti et al.[37] also reported through finite element analysis that the use of augments, regardless of type, alters femoral bone stress distribution, particularly in regions adjacent to the bone cut.

The finite element analysis demonstrated that, under different femoral bone defect locations, maximum interface micromotions remained within the accepted safety threshold regardless of augment use, and approximately 80-90% of femoral bone stresses were distributed within the reported reference range, showing satisfactory safety and stability.

Notably, when the bone defect was located at the medial condyle, the use of metal augment was associated with a more pronounced reduction in maximum interface micromotion and maximum femoral stress compared with other defect configurations. More importantly, in contrast to the effect observed with intramedullary stems, the use of metal augmentation increased the proportion of femoral bone

stress within the reference range. Specifically, the proportion of low-stress regions (<0.1 MPa) decreased from 17.20% to 15.88% with augment application, suggesting a reduced risk of stress shielding-related bone resorption. This effect is likely attributable to the increased bone-implant contact area provided by the metal augment and the redistribution of load toward the cancellous bone.

However, when bone defects were located at the lateral condyle or involved both condyles, metal augments did not show similar differences. This observation may be related to the asymmetric load distribution between the medial and lateral compartments of the knee, with the medial condyle generally subjected to higher physiological loading.

This study indicated that metal augments altered interface micromotion and stress distribution mainly in medial condylar defects, while their influence was overall limited. Across all configurations, acceptable micromotion levels and femoral stress distributions were achieved even without augments, suggesting that augments modify the local mechanical environment rather than being essential for initial femoral stability in this cementless RTKA system. Further experimental and clinical studies are also needed to clarify their role in different defect scenarios.

***Limitations***

This study has several limitations. First, only several predefined defect configurations with fixed geometry and depth were evaluated. More complex and irregular defect morphologies, particularly severe AORI type III defects, were not investigated and may exhibit different biomechanical behavior under the same reconstruction strategy.

Second, the analyses relied solely on finite element modeling without direct experimental biomechanical validation, and focused exclusively on initial mechanical stability. Bone remodeling, osseointegration processes, and long-term fatigue behavior of the implant-bone system were not considered, therefore, the conclusions should be interpreted with caution.

Third, the simulations were performed under simplified modeling assumptions and boundary conditions. The model was based on a single femoral geometry with homogeneous material properties, and did not include ligament forces, patellofemoral contact, or full dynamic gait loading. These simplifications may not fully represent the *in vivo* mechanical environment and may influence micromotion and stress distribution, thereby limiting generalizability.

## ***Conclusions***

In summary, this novel cementless RTKA system exhibited satisfactory femoral initial stability in the present finite element

model. Acceptable initial stability may be achieved without routine use of an intramedullary stem or metal augment in this system. However, given the model-specific assumptions and the focused scope of the present analysis, further experimental and clinical studies are required to validate these observations before drawing conclusions for broader surgical practice.

## References

1. Lei, P.-F., Hu, R.-Y. & Hu, Y.-H. Bone Defects in Revision Total Knee Arthroplasty and Management. *Orthop Surg* **11**, 15–24 (2019).
2. Schwartz, A. M., Farley, K. X., Guild, G. N. & Bradbury, T. L. Projections and Epidemiology of Revision Hip and Knee Arthroplasty in the United States to 2030. *The Journal of Arthroplasty* **35**, S79–S85 (2020).
3. Jm, T., Z, C., Gr, S. & Ma, M. The Epidemiology of Revision Total Knee Arthroplasty. *The journal of knee surgery* **34**, (2021).
4. Khan, Y., Arora, S., Kashyap, A., Patralekh, M. K. & Maini, L. Bone defect classifications in revision total knee arthroplasty, their reliability and utility: a systematic review. *Arch Orthop Trauma Surg* **143**, 453–468 (2023).
5. Rodríguez-Merchán, E. C., Gómez-Cardero, P. & Encinas-Ullán, C. A. Management of bone loss in revision total knee arthroplasty: therapeutic options and results. *EFORT Open Rev* **6**, 1073–1086 (2021).
6. Kang, S. G., Park, C. H. & Song, S. J. Stem Fixation in Revision Total Knee Arthroplasty: Indications, Stem Dimensions, and Fixation Methods. *Knee Surg Relat Res* **30**, 187–192 (2018).
7. Huff, T. W. & Sculco, T. P. Management of bone loss in revision total knee arthroplasty. *J Arthroplasty* **22**, 32–36 (2007).
8. Haidukewych, G. J., Hanssen, A. & Jones, R. D. Metaphyseal fixation in revision total knee arthroplasty: indications and techniques. *J Am Acad Orthop Surg* **19**, 311–318 (2011).
9. Restrepo, S., Smith, E. B. & Hozack, W. J. Excellent mid-term follow-up for a new 3D-printed cementless total knee arthroplasty. *Bone Joint J* **103-B**, 32–37 (2021).
10. Sultan, A. A. *et al.* Cementless 3D Printed Highly Porous

Titanium-Coated Baseplate Total Knee Arthroplasty: Survivorship and Outcomes at 2-Year Minimum Follow-Up. *J Knee Surg* **33**, 279–283 (2020).
11. Gallo, J., Goodman, S. B., Konttinen, Y. T., Wimmer, M. A. & Holinka, M. Osteolysis around total knee arthroplasty: a review of pathogenetic mechanisms. *Acta Biomater* **9**, 8046–8058 (2013).
12. Szoradi, G. T., Feier, A. M., Zuh, S. G., Russu, O. M. & Pop, T. S. Polymethyl Methacrylate Bone Cement Polymerization Induced Thermal Necrosis at the Cement–Bone Interface: A Narrative Review. *Applied Sciences* **14**, 11651 (2024).
13. Uivaraseanu, B. *et al.* Highlighting the advantages and benefits of cementless total knee arthroplasty (Review). *Exp Ther Med* **23**, 58 (2022).
14. O'Brien, S. *et al.* Prediction of backside micromotion in total knee replacements by finite element simulation. *Proc Inst Mech Eng H* **226**, 235–245 (2012).
15. Yang, H. *et al.* Validation and sensitivity of model-predicted proximal tibial displacement and tray micromotion in cementless total knee arthroplasty under physiological loading conditions. *J Mech Behav Biomed Mater* **109**, 103793 (2020).
16. Fonseca, F., Sousa, A. & Completo, A. Femoral revision knee Arthroplasty with Metaphyseal sleeves: the use of a stem is not mandatory of a structural point of view. *J Exp Orthop* **7**, 24 (2020).
17. Li, J., Tian, D., Yang, L., Zhang, J. & Hu, Y. Influence of a metaphyseal sleeve on the stress-strain state of a bone-tumor implant system in the distal femur: an experimental and finite element analysis. *J Orthop Surg Res* **15**, 589 (2020).
18. Wan, Q. *et al.* Appropriate sagittal positioning of femoral components in total knee arthroplasty to prevent fracture and loosening. *Bone Joint Res* **13**, 611–621 (2024).
19. Song, S. J., Kim, K. I. & Park, C. H. Comparison of the contact stress between the sensor and real polyethylene insert in total knee arthroplasty: a finite element analysis. *Ann Transl Med* **8**, 1424 (2020).
20. Du, M. *et al.* Tibio-Femoral Contact Force Distribution of Knee Before and After Total Knee Arthroplasty: Combined Finite Element and Gait Analysis. *Orthop Surg* **14**, 1836–1845 (2022).
21. Liu, Y. *et al.* Biomechanical comparison between metal block and cement-screw techniques for the treatment of tibial bone defects in total knee arthroplasty based on finite element analysis. *Computers in Biology and Medicine* **125**, 104006 (2020).
22. Zhao, G., Yao, S., Ma, J. & Wang, J. The optimal angle of screw for using cement-screw technique to repair tibial defect in total knee arthroplasty: a finite element analysis. *J Orthop Surg Res* **17**, 363

(2022).
23. Siddiqi, A., Chen, A. F., Piuzzi, N. S. & Kelly, M. A. The Use of Metaphyseal Cones and Sleeves in Revision Total Knee Arthroplasty. *JAAOS - Journal of the American Academy of Orthopaedic Surgeons* **29**, e904 (2021).
24. Carender, C. N. *et al.* Use of Cementless Metaphyseal Fixation in Revision Total Knee Arthroplasty in the United States. *J Arthroplasty* **37**, 554–558 (2022).
25. Li, Y., Wang, X. & Tian, H. Reconstruction for Massive Proximal Tibial Bone Defects Using Patient-Customized Three-Dimensional-Printed Metaphyseal Cones in Revision Total Knee Arthroplasty. *Orthop Surg* **14**, 1071–1077 (2022).
26. Remily, E. A. *et al.* Short-term Outcomes of 3D-Printed Titanium Metaphyseal Cones in Revision Total Knee Arthroplasty. *Orthopedics* **44**, 43–47 (2021).
27. Klim, S. M. *et al.* Excellent mid-term osseointegration and implant survival using metaphyseal sleeves in revision total knee arthroplasty. *Knee Surg Sports Traumatol Arthrosc* **28**, 3843–3848 (2020).
28. Wang, X. *et al.* Stability of Three-Dimensional Printed Custom-Made Metaphyseal Cone for Tibial Bone Defects Reconstruction: A Finite Element Analysis and Biomechanical Study. *Orthop Surg* **15**, 2937–2946 (2023).
29. Innocenti, B. Are Flexible Metaphyseal Femoral Cones Stable and Effective? A Biomechanical Study on Hinged Total Knee Arthroplasty. *The Journal of Arthroplasty* **39**, 1328–1334 (2024).
30. Murray, P. B., Rand, J. A. & Hanssen, A. D. Cemented long-stem revision total knee arthroplasty. *Clin Orthop Relat Res* 116–123 (1994).
31. Mihalko, W. M. & Whiteside, L. A. Stem pain after cementless revision total knee arthroplasty. *J Surg Orthop Adv* **24**, 137–139 (2015).
32. Cipriano, C. A., Brown, N. M., Della Valle, C. J., Moric, M. & Sporer, S. M. Intra-operative periprosthetic fractures associated with press fit stems in revision total knee arthroplasty: incidence, management, and outcomes. *J Arthroplasty* **28**, 1310–1313 (2013).
33. Completo, A., Fonseca, F. & Simões, J. A. Strain shielding in proximal tibia of stemmed knee prosthesis: experimental study. *J Biomech* **41**, 560–566 (2008).
34. Morgan-Jones, R., Oussedik, S. I. S., Graichen, H. & Haddad, F. S. Zonal fixation in revision total knee arthroplasty. *Bone Joint J* **97-B**, 147–149 (2015).
35. Senesi, G. *et al.* The relationship between stress shielding, bone density changes and implant migration, failure and fracture after

total knee arthroplasty: A systematic review. *J Exp Orthop* **12**, e70350 (2025).
36. Vasso, M., Beaufils, P., Cerciello, S. & Schiavone Panni, A. Bone loss following knee arthroplasty: potential treatment options. *Arch Orthop Trauma Surg* **134**, 543–553 (2014).
37. Innocenti, B., Fekete, G. & Pianigiani, S. Biomechanical Analysis of Augments in Revision Total Knee Arthroplasty. *J. Biomech. Eng.-Trans. ASME* **140**, 111006 (2018).

**Figure legends**

**Figure 1**. The design of the cementless RTKA system (A: the femoral RTKA system; B: the femoral metaphyseal cone)

**Figure 2**. The assembly of the femur-prosthesis.

**Figure 3**. Effects of an intramedullary stem on the initial stability in the absence of bone defects.

1. Micromotions between the porous layer of the femoral metaphyseal cone and the femur (a-stemless; b-stem).

2. Micromotions between the distal femoral condylar component and the femur (a-stemless; b-stem)

3. von Mises equivalent stress of the femur (a-stemless; b-stem)

Figure 4. Effects of intramedullary stem on initial stability in the presence of severe bone defects.

1. Micromotions in case of medial-lateral bone defects (a-stemless; b-stem)

2. Micromotions in case of medial bone defects (a-stemless; b-stem)

3. Micromotions in case of lateral bone defects (a-stemless; b-stem)

4. von Mises equivalent stress of the femur in case of medial-lateral bone defects (a-stemless; b-stem)

5. von Mises equivalent stress of the femur in case of medial bone defects (a-stemless; b-stem)

6. von Mises equivalent stress of the femur in case of lateral bone defects (a-stemless; b-stem)

**Figure 5**. Effects of augments on the initial stability in the presence of severe bone defects.

1. Micromotions between the porous layer of the femoral metaphyseal cone and the femur in case of medial-lateral bone defects (a-no augment; b-augment)

2. Micromotions between the porous layer of the femoral metaphyseal cone and the femur in case of medial bone defects (a-no augment; b-augment)

3. Micromotions between the porous layer of the femoral metaphyseal cone and the femur in case of lateral bone defects (a-no augment; b-augment)

4. von Mises equivalent stress of the femur in case of medial-lateral bone defects (a-no augment; b-augment)

5. von Mises equivalent stress of the femur in medial bone defect (a-no augment; b-augment)

6. von Mises equivalent stress of the femur in lateral bone defect (a-

no augment; b-augment)

## Declarations

### *Ethics approval and consent to participate*

The study was approved by Peking University Third Hospital Medical Science Research Ethics Committee (M2021636). All procedures involving human participants were conducted in accordance with the Helsinki Declaration. Informed consent was also obtained from the participant in this study.

### *Consent for publication*

Consent for publication of the patient's clinical details and related images was obtained from the participant.

### *Availability of data and materials*

The datasets used or analyzed during the current study are available from the corresponding author on reasonable request.

### *Competing interests*

All the authors declare that they have no conflict of interest.

### *Acknowledgement*

Not applicable

### *Funding*

Funding support was provided from Beijing Natural Science

Foundation (23G12187, L254010)

***Authors' contribution***

Ziyang Dong and Xinguang Wang contributed equally to this work. Ziyang Dong and Xinguang Wang analyzed the data, interpreted the results, and drafted the main manuscript. Dongyang He, Xiaofan Lv, Ti Zhang, and Zijian Li contributed to the construction, analysis, and verification of the finite element analysis (FEA) model Xiaogang Zhang and Hua Tian provided supervision, conceptual guidance, and administrative support. All authors reviewed and approved the final version of the manuscript.

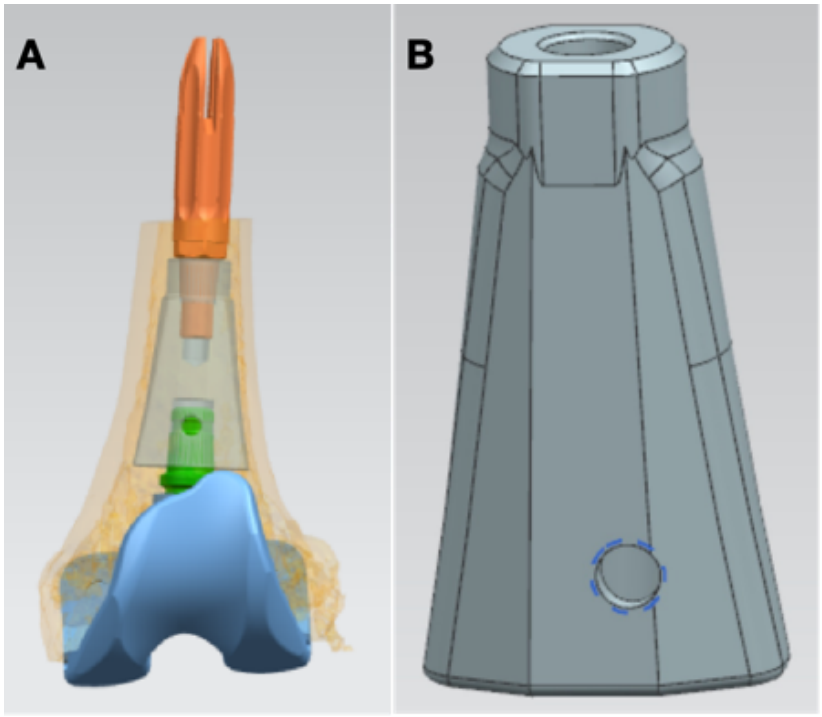


Figure 1. The design of the cementless RTKA system (A: the femoral RTKA system; B: the femoral metaphyseal cone)

Figure 2. The assembly of the femur-prosthesis.

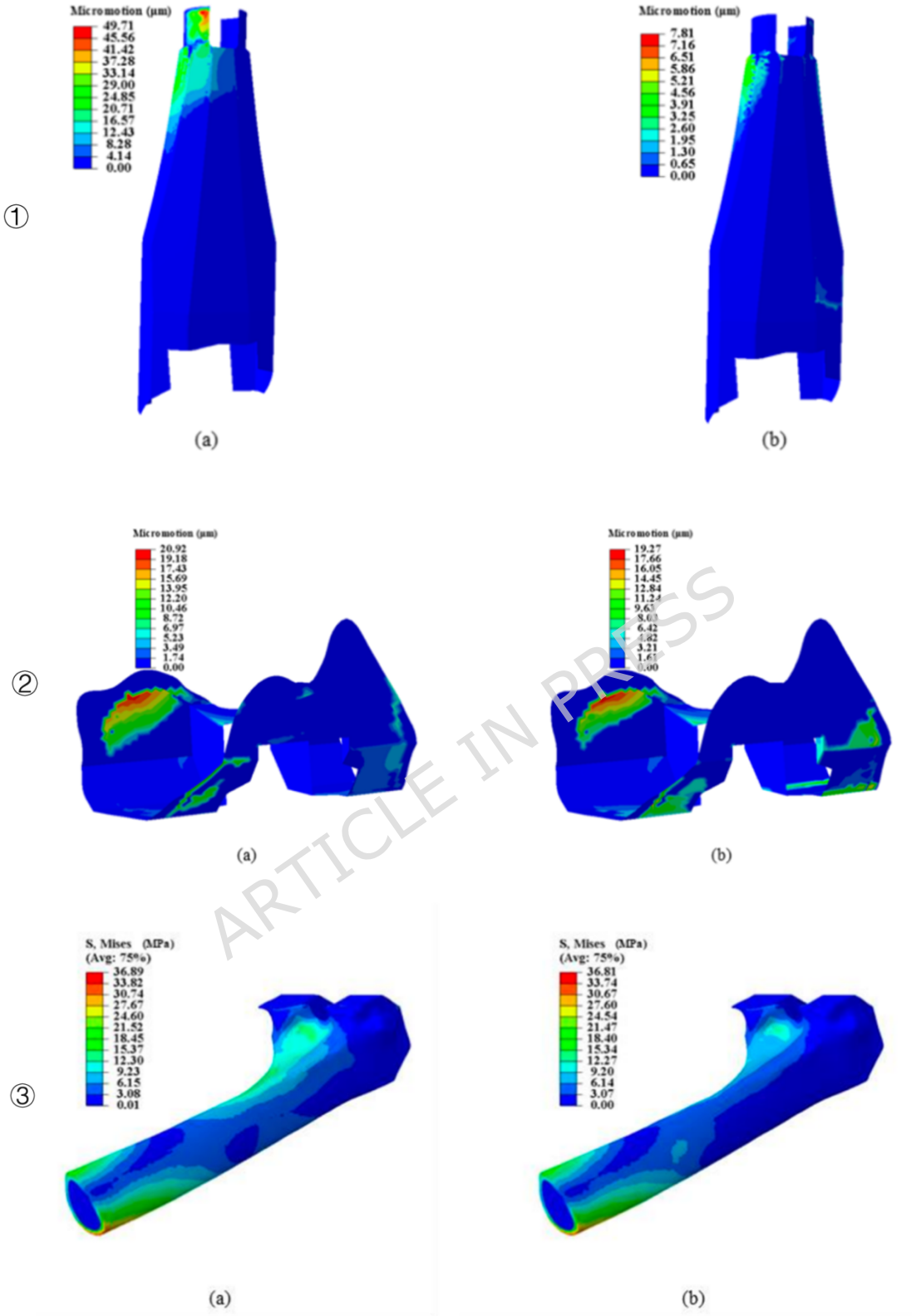


Figure 3. Effects of an intramedullary stem on the initial stability in the absence of bone defects.

1. Micromotions between the porous layer of the femoral metaphyseal cone and the femur (a-stemless; b-stem).

2. Micromotions between the distal femoral condylar component and the femur (a-stemless; b-stem)

3. von Mises equivalent stress of the femur (a-stemless; b-stem)

①

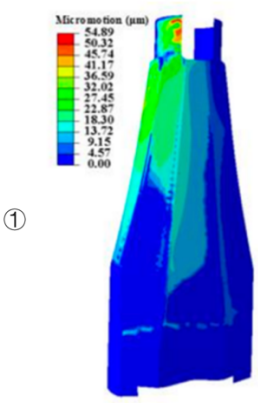


(a)

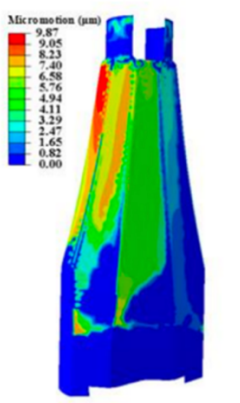


(b)

②

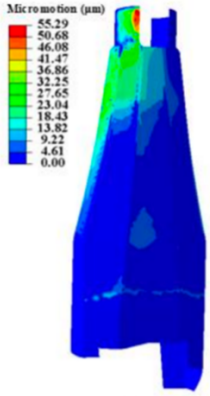


(a)

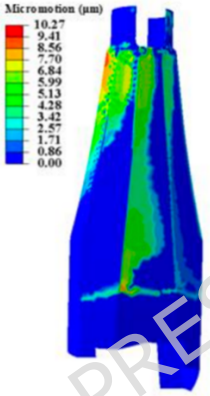


(b)

③

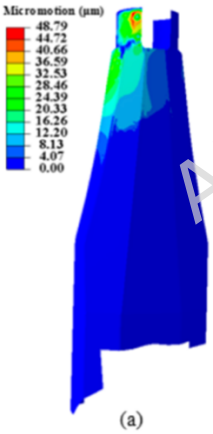


(a)

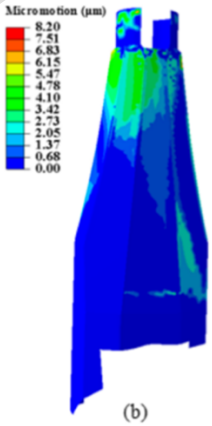


(b)

④

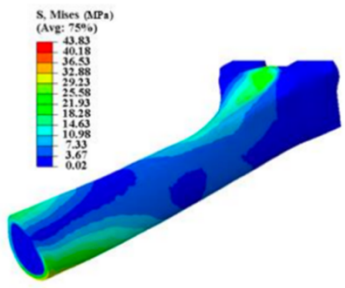


(a)

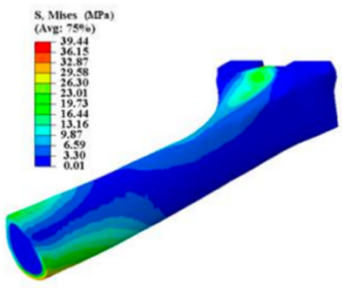


(b)

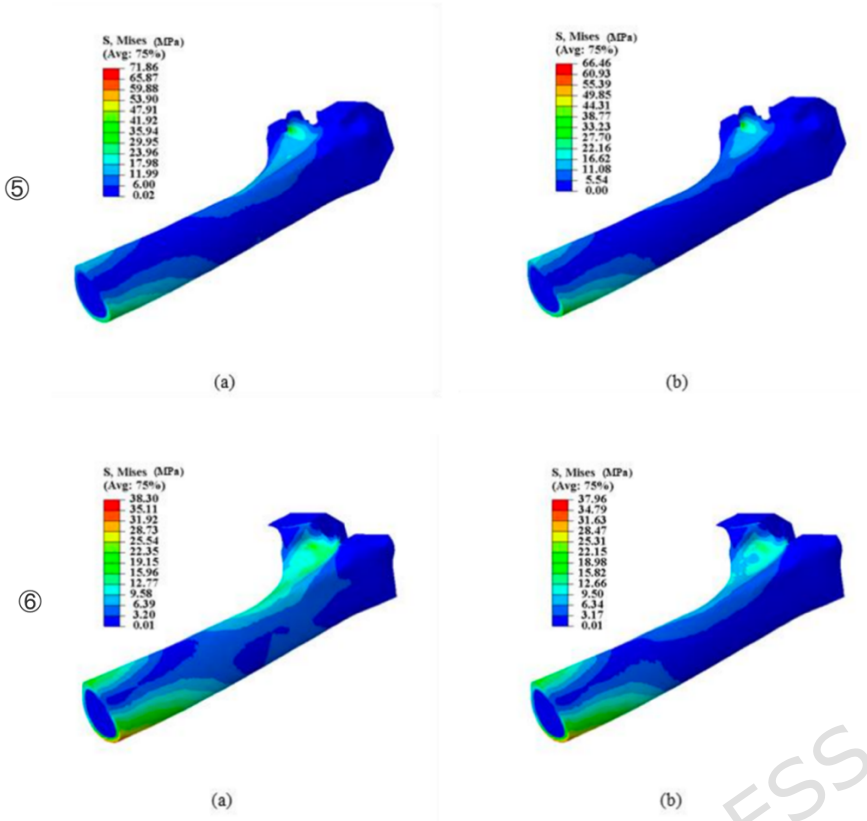


Figure 4. Effects of intramedullary stem on initial stability in the presence of severe bone defects.

1. Micromotions in case of medial-lateral bone defects (a-stemless; b-stem)

2. Micromotions in case of medial bone defects (a-stemless; b-stem)

3. Micromotions in case of lateral bone defects (a-stemless; b-stem)

4. von Mises equivalent stress of the femur in case of medial-lateral bone defects (a-stemless; b-stem)

5. von Mises equivalent stress of the femur in case of medial bone defects (a-stemless; b-stem)

6. von Mises equivalent stress of the femur in case of lateral bone defects (a-stemless; b-stem)

①

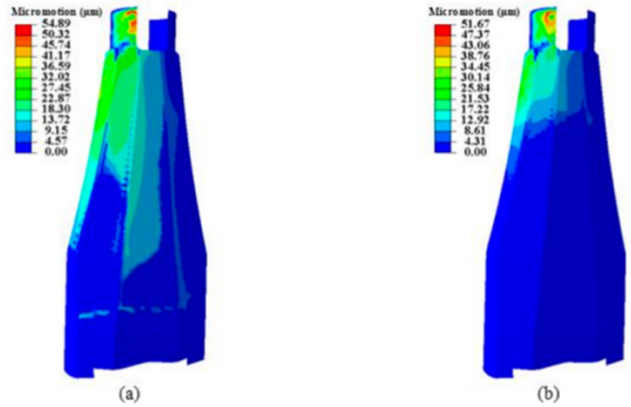


②

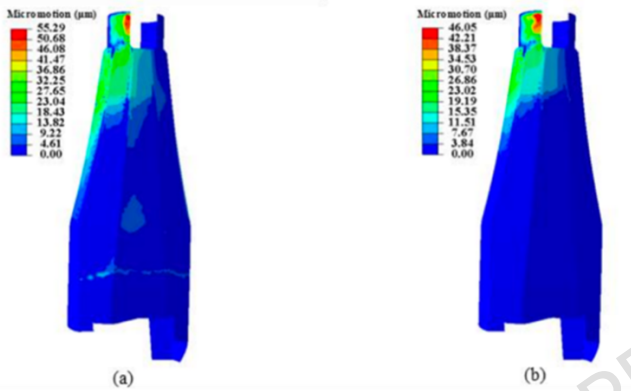


③

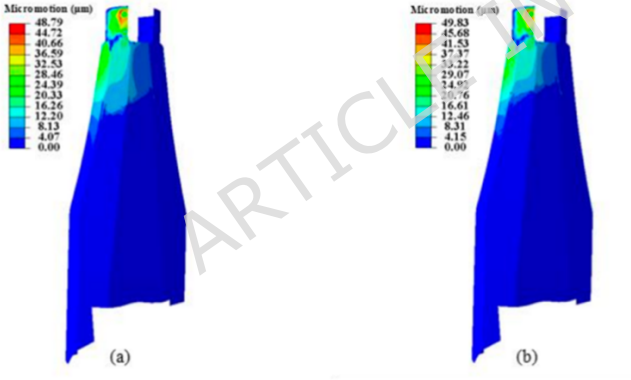


④

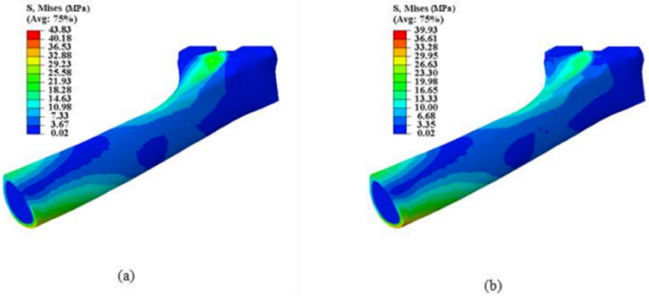

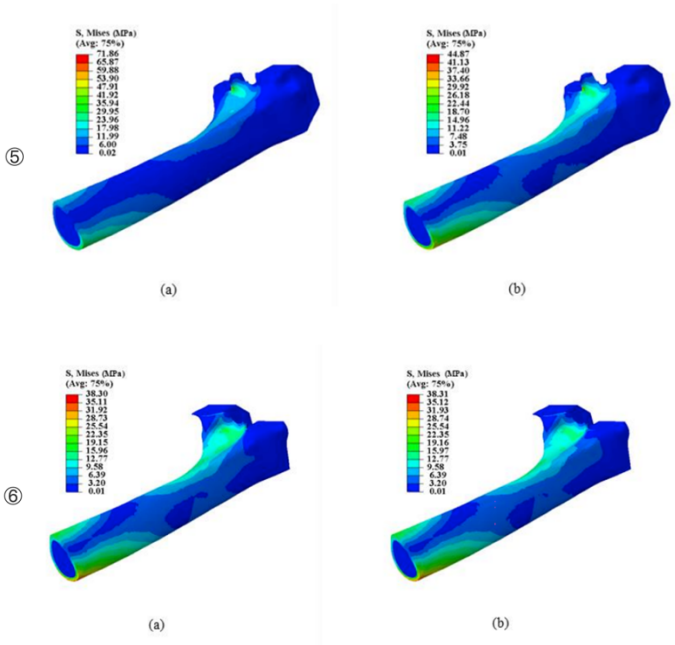


Figure 5. Effects of augmentations on the initial stability in the presence of severe bone defects.

1. Micromotions between the porous layer of the femoral metaphyseal cone and the femur in case of medial-lateral bone defects (a-no augment; b-augment)

2. Micromotions between the porous layer of the femoral metaphyseal cone and the femur in case of medial bone defects (a-no augment; b-augment)

3. Micromotions between the porous layer of the femoral metaphyseal cone and the femur in case of lateral bone defects (a-no augment; b-augment)

4. von Mises equivalent stress of the femur in case of medial-lateral bone defects (a-no augment; b-augment)

5. von Mises equivalent stress of the femur in medial bone defect (a-no augment; b-augment)

6. von Mises equivalent stress of the femur in lateral bone defect (a-no augment; b-augment)